

Alpha/beta-gated gamma-gamma spectroscopy of mixed fission products for trace analysis

Bruce D. Pierson¹ • Brian C. Archambault¹ • Lawrence R. Greenwood¹ • Morgan M. Haney¹ • Michael G. Cantaloub¹ • Alex R. Hagen¹ • Staci M. Herman¹ • Nicolas E. Uhnak¹ • James M. Bowen¹ • Jane H. Estrada¹

Received: 1 July 2022 / Accepted: 1 October 2022

This is a U.S. Government work and not under copyright protection in the US; foreign copyright protection may apply 2022

Abstract

Dissolved fission product samples were analyzed using advanced radio-emission spectroscopy techniques using a proof-of-concept instrument. Reduction factors of 2–7 in the minimum detectable activity relative to traditional gamma counting were observed for trace fission products and actinides. A gamma-gamma coincidence detector was combined with a custom liquid scintillation counter to evaluate the benefits of alpha and beta coincident and anti-coincident analysis. The improvements observed in the detection sensitivity of fission products and actinides achieved by combining time-correlated radiation signatures is of value to applications such as nuclear physics, environmental monitoring, reactor releases, and nuclear forensics.

 $\textbf{Keywords} \ \ Radiation \ detection \cdot Coincident \ radiation \ spectroscopy \cdot Charged-particle \ coincidence \ counting \cdot Fission \ products$

☑ Bruce D. Pierson bruce.pierson@pnnl.gov

Brian C. Archambault brian.archambault@pnnl.gov

Lawrence R. Greenwood larry.greenwood@pnnl.gov

Morgan M. Haney morgan.haney@pnnl.gov

Michael G. Cantaloub m.cantaloub@gmail.com

Alex R. Hagen alexander.hagen@pnnl.gov

Staci M. Herman staci.herman@pnnl.gov

Nicolas E. Uhnak nicolas.uhnak@pnnl.gov

James M. Bowen james.bowen@pnnl.gov

Jane H. Estrada jane.estrada@pnnl.gov

Published online: 08 November 2022

Pacific Northwest National Laboratory, P.O. Box 999, Richland, WA 99354, USA

Introduction

Beta/gamma and gamma-gamma coincident radiation spectroscopy techniques are used to study the decay schemes of single isotopes and conduct low-level counting. Decayscheme measurements are made using a known single-isotope standard or purified ion beams with an absolute atom count made using ion current or absolute beta counting as the atom basis for measurements of short-lived isotopes. The use of alpha/beta coincident counting methods is less common, in part, because evaluating the data from mixed analyte samples using these and other more advanced radioemission spectroscopy techniques is difficult. Multi-detector instruments require custom data acquisition systems and lack commercial resources to interpret the data. Furthermore, few full-featured analysis resources are commercially available that provide the necessary quality assurance pedigree. These technical challenges and few practical applications limit the widespread adoption of coincident spectroscopy. Application requirements ultimately drive incentives for more prolific use of different techniques.

Refinements in nuclear physics modeling, particularly in actinide fission theory, are in need of more sensitive analysis techniques to expand the number of measured fission product yields. In addition to fundamental nuclear physics, select national security applications need faster, more sensitive



analysis techniques as well, warranting a review of current capabilities and benefits that alpha/beta coincident gamma spectroscopy may provide to the analysis of mixed fission product (MFP) samples.

In this manuscript, the benefits of alpha/beta-gated, gamma-gamma coincidence counting applied to a MFP sample acquired 8-days post irradiation for isotope identification and quantification will be presented. Improvements in detection sensitivity and methods for optimizing the detection limit for weaker trace analytes is also discussed. More than 22 separate alpha, beta, and gamma emitting radionuclides were present in the sample, of which eight typically require chemical isolation for radiometric quantification using traditional high-purity germanium (HPGe) assay.

Background

Coincidence spectroscopy techniques have been used to reduce background, avoid interferences, and improve detection sensitivity for decades and are used regularly in nuclear astrophysics for quantifying trace activities of primordial positron emitters [1, 2]. Cosmic and terrestrial background sources can interfere, shroud, or reduce the accuracy of measurements, especially where the coincident emission of two 511 keV gammas from positron annihilation is the primary signature like ²⁶Al and ²²Na.

Instruments using fundamentally similar methods to those presented in this manuscript are in use today and measure decay transition lifetimes on the order of nanoseconds using fast scintillating gamma detectors [3]. The beta-gamma-gamma coincident instrument in use at the Kyoto University Reactor-Online Isotope Separator (KUR-ISOL) makes use of a LaBr₃ scintillator, a HPGe detector, and a plastic scintillator to estimate nuclear level transition times using the scintillators and gating on specified transitions using the energy resolution of the HPGe detector.

Variations on alpha- and beta-gated gamma spectroscopy have been demonstrated as a useful method for reducing environmental background by orders of magnitude [1, 4, 5]. Improved detection sensitivity to fission products is a crosscutting need, valuable to the nuclear physics, safeguards, treaty verification, and forensics communities. Problems within these communities are complex, relying on many signatures to inform scientifically-derived conclusions. Several fission products have low-probability gamma transitions (91Y), small fission yields (156Eu, 161Tb), weak specific activity (137Cs), or combinations thereof. These characteristics make it difficult to quantify directly from MFP samples using convenient, cost-effective techniques like gamma-ray spectroscopy. Isotopes, like ⁸⁹Sr, ⁹¹Y, ¹¹¹Ag, ¹¹⁵Cd, ¹³⁶Cs, ¹³⁷Cs, ¹⁵³Sm, ¹⁵⁶Eu, and ¹⁶¹Tb, commonly require chemical separation to quantify from a MFP sample [6–9]. Others,

like ¹⁵⁶Sm, ¹⁴⁹Nd, ¹⁵¹Pm, ¹¹³Ag, ¹²⁸Sb, ¹⁴⁵Pr, ⁷⁷Ge/As, and ⁸²Br, are short-lived, making chemical purification time sensitive. Accessing all of the fission products directly from unseparated samples requires better detection sensitivities and more sophisticated radiometric analysis techniques.

Experimental

On February 21st, 2020, a sample of 93% highly enriched uranium (HEU) was irradiated with thermal neutrons in the center core flux trap of the Massachusetts Instituted of Technology reactor for 12,000 s starting at 6:14 PST. The sample was shipped to Los Alamos National Laboratory and dissolved using 4 M HNO₃. A fraction of the dissolved material was transferred to Pacific Northwest National Laboratory (PNNL) for chemical separation and analysis. A fraction of the material was analyzed by the PNNL service center. This service center includes state-of-the-art gamma-ray and mass spectrometry facilities that commonly perform qualityassured analysis of samples for environmental monitoring as part of the Hanford nuclear waste site cleanup. The analysis results of the gamma spectroscopy and radiochemical analysis of this sample by the PNNL service center were used as the reference for the analysis conducted using the newly commissioned Gamma-Alpha-Beta Radio-Isotope EvaLuator (GABRIEL) detector[10]. The analytical support operation service center at PNNL conforms to the Hanford Analytical Service Quality Assurance Requirements Documents (HASQARD) [11].

This service center determined that there were 3.33E + 12(+/-4%) fissions from ²³⁵U/g of solution contained in the sample received by PNNL. All sample preparation was subsequently performed gravimetrically. Added uncertainty from sample preparation has been historically evaluated to be comparable to the scale uncertainty. An aliquot of 0.0309(4) g (equivalent to approximately 1E+11 fissions) of the original sample in 4 M HNO₃ was brought to near dryness and transposed twice with 0.5 mL of optima grade concentrated HCl. The aliquot was subsequently brought to near dryness before reconstituting the material in 1 mL of 0.55 M HCl. After the sample was fully transposed, 9 mL of UltimaGold A/B liquid scintillation cocktail was added. The sample was inverted several times to complete mixing.

Data were collected from two matched 50% relative-efficiency Ortec GMX-50200-S *n*-type coaxial HPGe detectors and two R11265U-200 Hamamatsu photo-multiplier tubes (PMTs) time-synchronously. The instrument was assembled inside of a square cubic foot volume inside a graded gamma spectroscopy lead shield. The instruments were connected to two CAEN digitizers: a DT5781 digital multi-channel analyzer for the HPGe detectors, and a DT5730 waveform



digitizer for the two PMTs. Both digitizers were synchronized to a common clock using a DT4700 clock pulse generator. A diagram of the setup is presented in Fig. 1. The blue wires indicate the clock synchronization cables, orange the signal trace cables for the PMTs, and black signal trace from the HPGe detectors.

The DT5781 performed trapezoidal shaping using the digital pulse processing-pulse height analysis (DPP-PHA) firmware version 4.19_128.71; a 6 µs shaping time and 1 µs flat top were used to collect the data. The DT5730 used the DPP-pulse shape discrimination (DPP-PSD) firmware version 4.17_136.16. A 160 ns pulse integration window was used with an 18 ns pre-trigger start and a 24 ns short integration time. Figure 2 illustrates how the provided PSD constants translate to pulses from the PMTs. A standard method of PSD leveraging the ratio of the peak

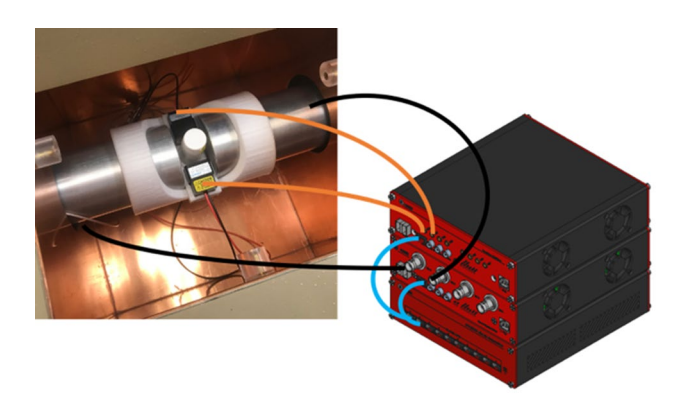


Fig. 1 A depiction of the digital acquisition and detector configuration. (colour figure online)

coong the modern PHA) siting and coor

area integration to the total area (sum of short and long window) was used to separate the alphas and betas.

Alpha radiolysis is a high linear energy transfer (LET) interaction. Most of the kinetic energy of the alpha particle is deposited into a few molecules of the fluorescing cocktail relative to betas. This type of interaction produces more ionization relative to excitation. Alpha energy deposition within the fluor molecules in the liquid scintillation cocktail produce more electron-ion pairs in close proximity. These charged pairs produce more triplet bound states during recombination. Triplet states transfer their excess energy between adjacent fluors to produce delayed photon emissions [12]. The extended lifetime and delayed interaction of triplet states produces delayed photons from subsequent singlet states that are observed as small afterpulses following the primary pulse. The region following the primary pulse in green of Fig. 2 is physically related to the ionization potential of the incident interacting particle and was used to discriminate between alphas and betas in this work.

A NIST-traceable multi-nuclide standard was counted a priori to characterize the HPGe detector performance. Figure 3 presents the measured full-energy peak efficiencies for the two HPGe detectors along with a plot of the fitted efficiency residual. Radionuclides with gamma emission energies outside of the calibrated energy range were not used to avoid the use of extrapolation in the efficiency fit.

Fig. 2 Example oscilloscope trace of an alpha scintillation event with after-pulsing. The black region represents the baseline, red the event pulse, and green the post-pulse trace. (colour figure online)

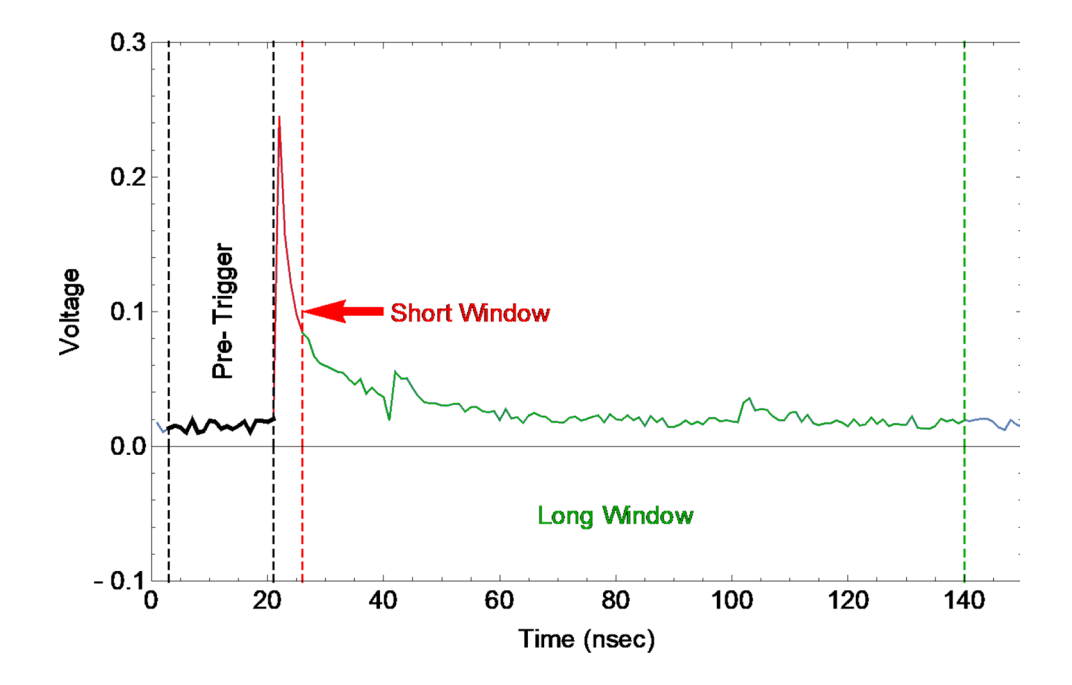
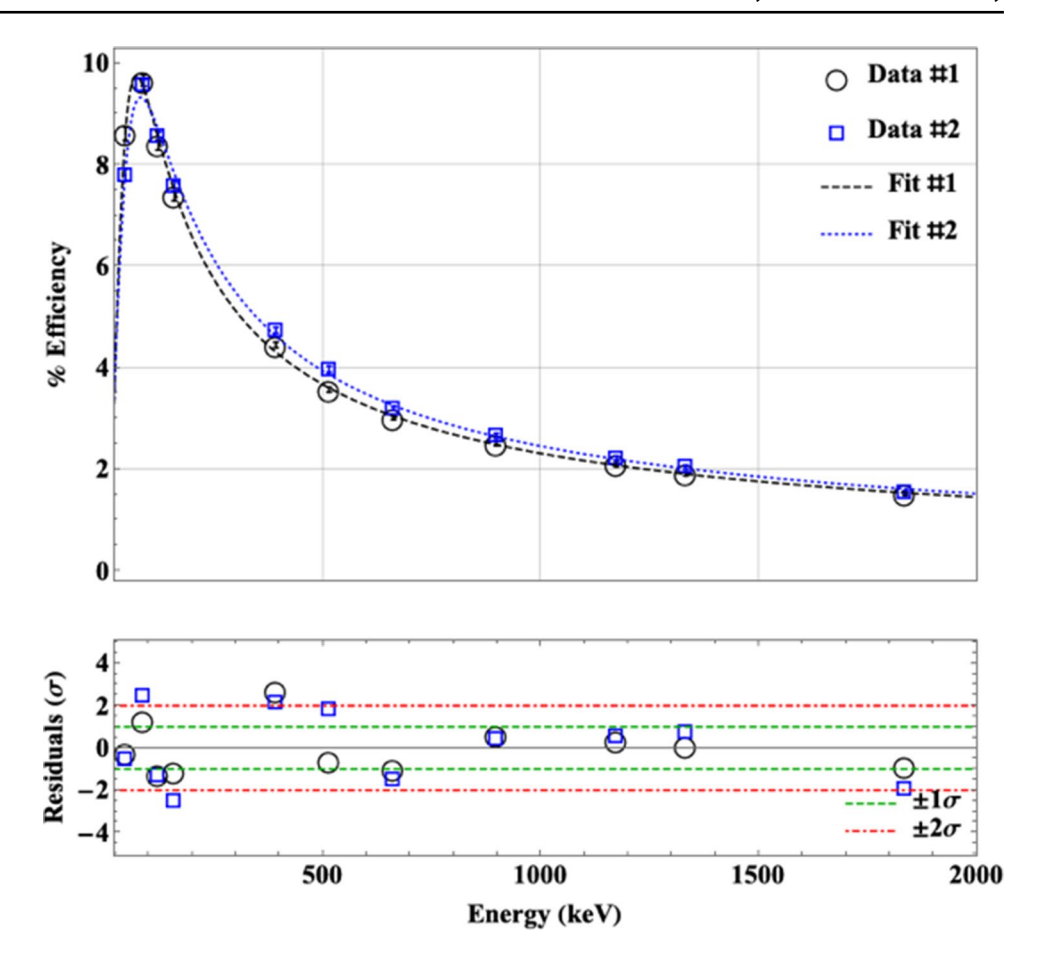




Fig. 3 Measured full-energy peak detection efficiency for the two HPGe detectors



Data and analysis

Data from each detector within the GABRIEL system were recorded in separate files using a serial event binary format with start of acquisition corresponding to time-zero. Each event was composed of two short integers representing the board and channel number, followed by a 64-bit ps resolution time-stamp, two short integers representing the analog-to-digital (ADC) energy bin number and DPP-PSD short integration window ADC bin number, and a 32-bit flag describing the type of event. The flash ADC accumulated digital representations of each pulse transient exceeding a user-defined threshold and performed both a fast differential and long shaping analyses to classify each event for precision dead-time estimates.

The raw list-mode data were parsed and stored using CERN's ROOT data analysis C++ framework for easier manipulation, visualization, and analysis [13]. Binary datasets from each detector were post-processed to reconstruct the coincident data sets. A sorted nearest neighbor search was conducted between detectors using the time differences within the search to build separate coincident datasets. The time-sorted nearest neighbor search cross-checked paired events within the list against adjacent events to avoid double

counting coincident events, only storing paired events in closest proximity. A graphical example is provided in Fig. 4.

Beta detector characterization

The beta detector energy and efficiency calibration were estimated using peak area ratios between the PMT gated and ungated HPGe spectra. Table 1 shows the fission products and their respective beta-correlated gamma signatures used to characterize the LSC counter. Most of the fission products used to measure the β efficiency have multiple energies. However, the predominant β -energy feeding the gamma level transition makes up the majority of the associated betas when inspecting the ratio of a primary gamma-line using beta-coincidence counting. Although not perfect, this ratio can be treated as a reasonable surrogate for a single β -energy efficiency measurement.

Peak areas between the beta-gated and ungated spectrum were used to internally calibrate the custom LSC. The beta detection efficiency did not exceed ~93% at peak energies and decreased to a minimum of ~20% for low-energy $\beta_{\rm max}$. Figure 5 depicts the best estimate of the beta detection efficiency as a function of beta end-point energy.



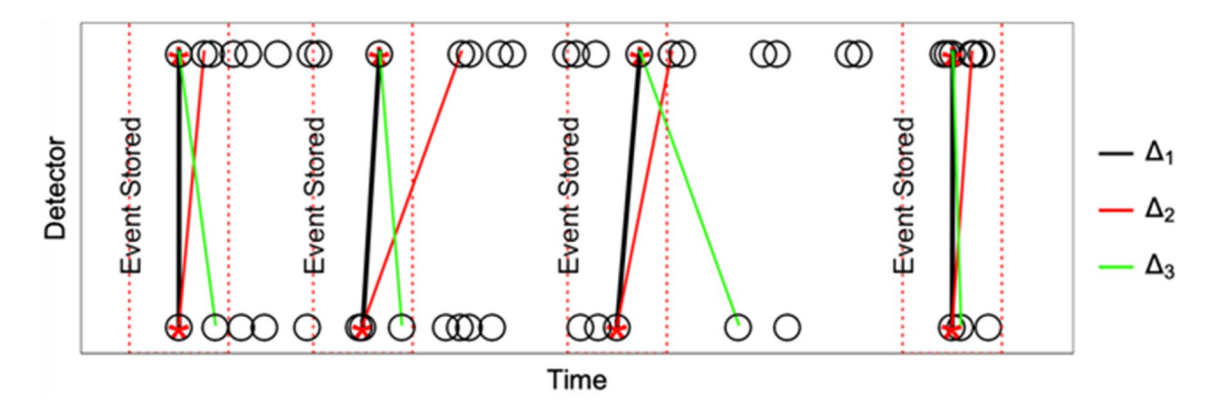


Fig. 4 Graphical demonstration of nearest-neighbor matching algorithm used to post-process and reconstruct coincident datasets from the HPGe detectors and LSC. Time differential sets are intercom-

pared with different forward differences depicted in red and green and the stored event in black. (colour figure online)

Table 1 Gamma-line ratios and associated beta end-point energies used to estimate the beta detection efficiency as a function of energy

Fission product	Gamma energy (keV)	Energy β_{max} (keV)
⁹⁵ Nb	765.8	159.8
⁹⁵ Zr	756.7	366.9
¹³² Te	228	240
¹⁴⁷ Nd	91	804.9
¹⁴⁷ Nd	531	365
¹⁴⁴ Ce	133.5	185.2
¹⁴¹ Ce	145.4	435
¹⁴³ Ce	293.3	111.3
⁹⁹ Mo	739.5	437.2
⁹⁹ Mo	181	437.2
¹⁴⁰ Ba	537.3	466

Beta spectra associated with select gamma-gamma coincidences were used to estimate the LSC energy calibration. Figure 6 depicts the best estimate of the beta energy calibration as a function of beta end-point energy and Table 2 lists the endpoint beta-energy associated with select coincident transitions.

Mixed fission product (MFP) spectra

Elements with atomic numbers from zinc to dysprosium, and everything in-between, are produced by fission. Hundreds of radionuclides and isomers are accumulated in the sample, many with short half-lives. In MFP samples, isotopes decay along their respective isobar decay chains until only the longer-lived (half-lives on the order of days) daughter radionuclides remain. Many of these radionuclides can be directly quantified using traditional gamma counting techniques [14]

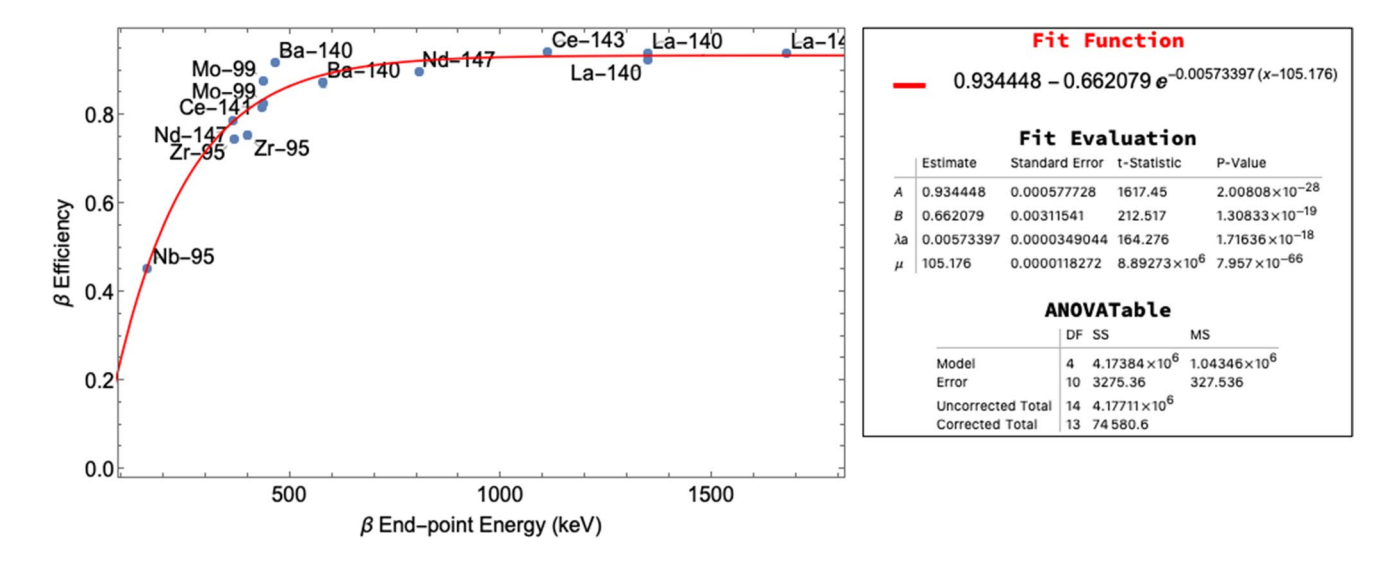


Fig. 5 Estimate of beta detection efficiency as a function of beta end-point energy in keV

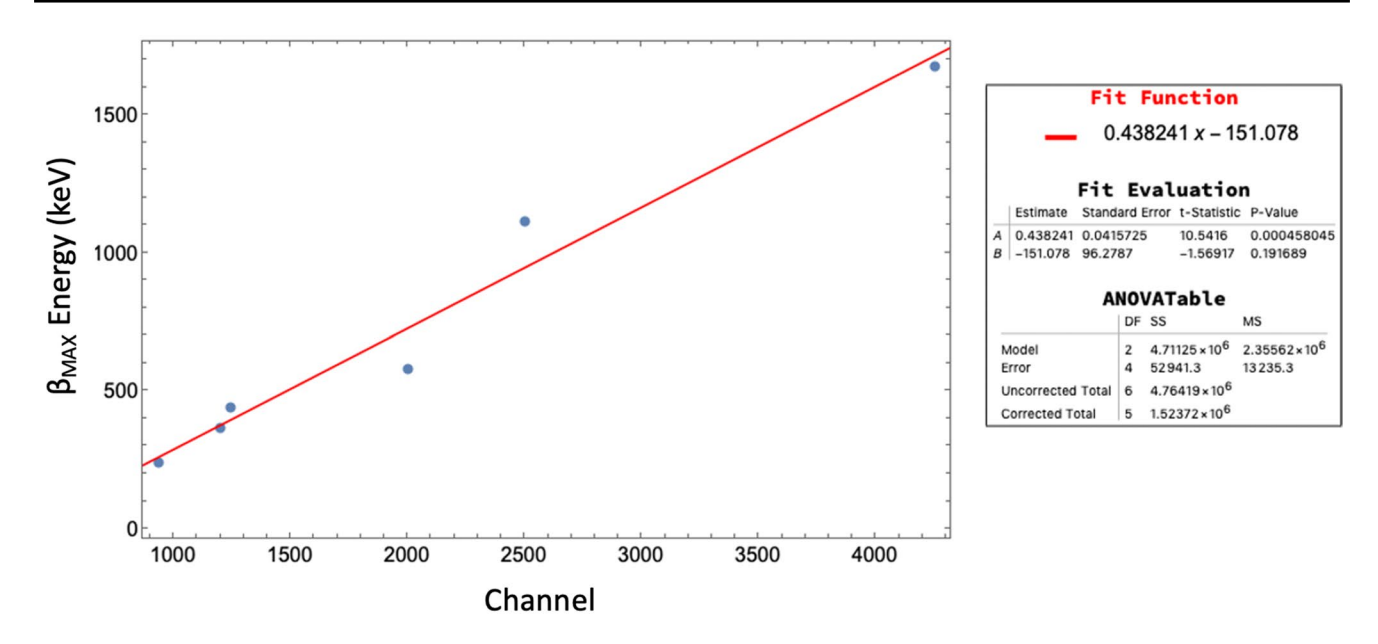


Fig. 6 Estimate of beta LSC calibration as a function of beta end-point energy

Table 2 Gamma-gamma transitions used to estimate the beta energy calibration

Fission product	Gamma-pair (keV)	Energy β_{max} (keV)
¹⁴⁰ La	487/1596	1676.9
⁹⁹ Mo	739/181	437.2
¹⁴⁰ Ba	304/162	579
¹³² Te	228/50	240
¹⁴³ Ce	293/57	1111.3
¹⁴⁷ Nd	319/91	365

like ⁹⁵Zr/Nb, ⁹⁷Zr, ⁹⁹Mo, ¹⁰³Ru, ¹³²Te/I, ¹⁴¹Ce, ¹⁴³Ce, and ¹⁴⁴Ce, and ¹⁴⁷Nd. Figure 7 depicts the measured gamma spectrum with and without beta-gating and with alphagating for reference. Other radionuclides, like ⁹¹Y, ¹¹¹Ag, ¹¹⁵Cd, ¹³⁶Cs, ¹³⁷Cs, ¹⁵³Sm, ¹⁵⁶Eu, and ¹⁶¹Tb, are not quantified directly with high accuracy from MFP using traditional gamma-ray spectroscopy because of Compton shadowing and gamma-ray interferences.

The datasets from the four detectors were parsed and stored as ROOT TTree objects. Post-acquisition coincident datasets were generated between the two PMTs first. Liquid scintillation counting is commonly performed using two PMTs operating in coincidence to reduce the dark current background. The coincident PMT data set was then

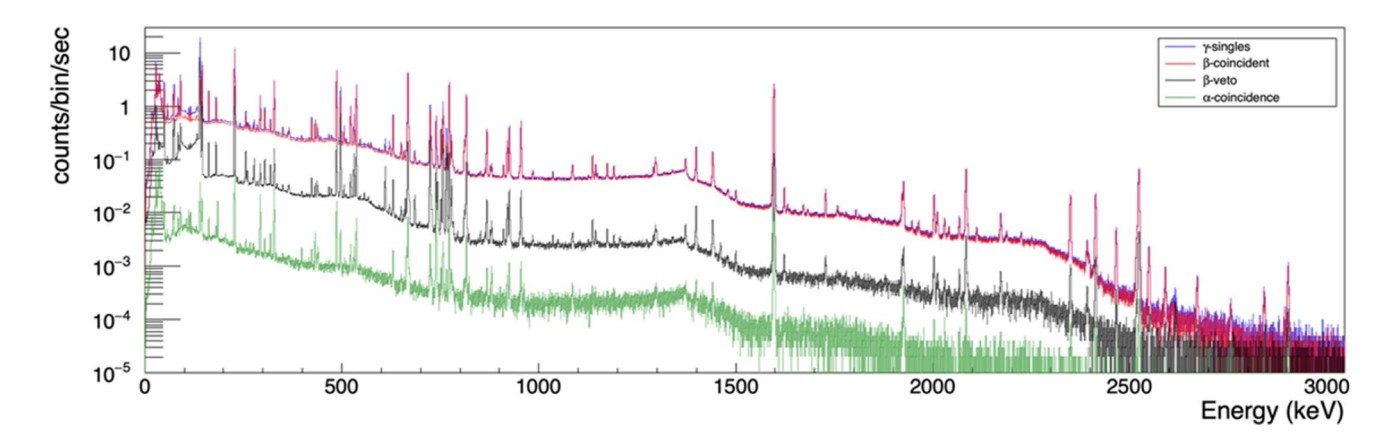


Fig. 7 Measured gamma spectrum of the mixed fission product sample with and without beta gating (blue/red), beta veto (black), and alpha gating (green). The channel space width was 0.2 keV/channel. (colour figure online)



used to generate the PMT/gamma coincident datasets for each HPGe detector. A coincident dataset between the two HPGe detectors was then produced and subsequently used with the coincident PMT dataset to generate a PMT/gamma-gamma coincident dataset. Log-plots of the time-difference between the two PMTs, the PMTs and one of the HPGe detectors, and between the two HPGe detectors are provided in Figs. 8, 9, 10, respectively.

More than 99% of all events depicted in Fig. 8 were recorded within a 100 ns time window (\pm 50 ns from 0). The remainder of the events are likely associated with coincidences between high-energy beta decay events registered in one PMT and small after pulses or conversion electron emissions registered in the second PMT.

The timing distribution presented in Fig. 9 is more interesting. The large peak occurs at ~ 1000 ns because the time difference plotted is the difference between the beta and the HPGe event time, which more often occurs after the PMT fires and represents 99.7% of all events. Figure 10 illustrates the traditional timing distribution observed between two matched germanium detectors.

Results and discussion

Alpha- and beta-correlated radiation signatures were acquired and studied to quantify the improvements to the detection limit for fission products and actinides. Cases where there was improvement for an observed gammaline were compared based on statistical quantification and/or MDA. The MDA used is based on the Currie method described in the Mirion Genie2000 Customization Tools Manual.

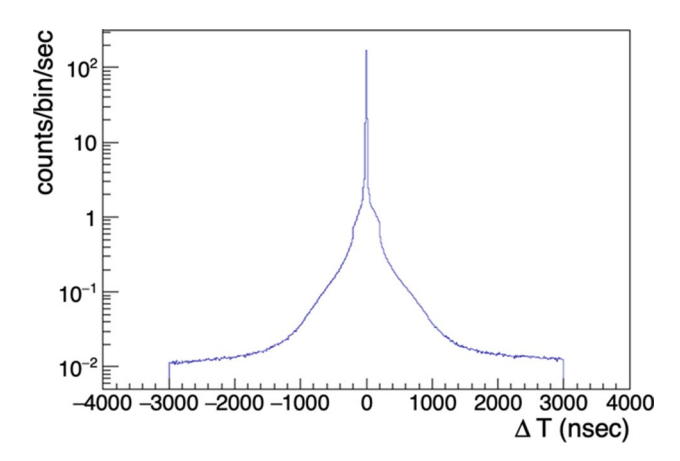


Fig. 8 Time-differential measured from the two PMTs used in the LSC counter (bin width is 10 ns)

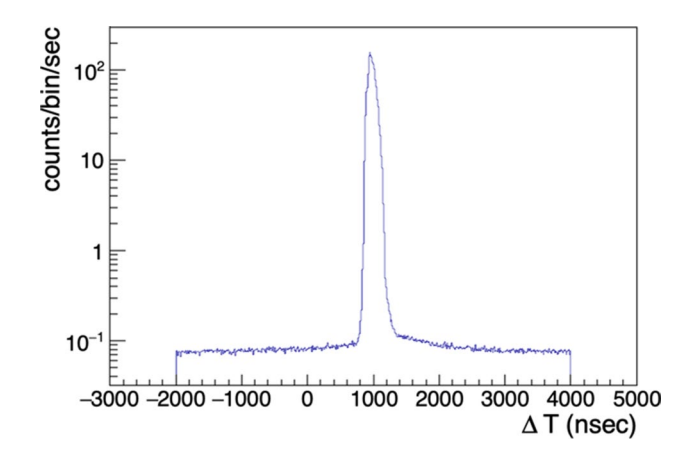


Fig. 9 Time-differential measured between coincident PMT light events and one of the HPGe detectors (bin width is 10 ns)

Quantified analytes

Spectra acquired from MFP samples often contain hundreds of separate and overlapping gamma signatures; many of which can be attributed to the same radionuclide. For example, ¹⁴⁰La and ¹³²I have more than 20 prominent gammalines each that can be directly observed in MFP samples. A list of primary gamma energies useful for quantification of various fission products and measured results as compared to PNNL's service center measurements is provided in Table 3. A total of 3.33E + 12 fissions/g of stock solution was measured using these prominent fission product and associated fission yields.



The ⁹¹Y gamma transition occurs in rapid succession with the emitted beta. Virtually no reduction in background is achieved by only processing gammas coincident with

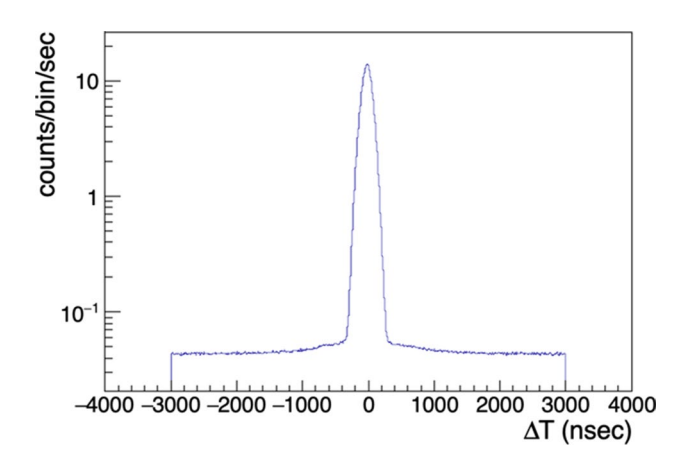


Fig. 10 Time-differential measured between the two HPGe detectors (bin width is 10 ns)



Table 3 Inter-comparison of measured results by traditional gamma counting and radiochemistry to results derived from GABRIEL

Isotope	Gamma-line (keV)	PNNL atoms/g	+/- %	GABRIEL atoms /g	+/-	Ratio
⁹¹ Y	1204	1.89E+11	5.8	2.05E+11	5.0	1.08
95mNb	236	_		1.27E+11	2.0	_
95 Zr	756	2.16E + 11	2.0	2.07E + 11	2.0	0.96
97 Zr	743	2.04E + 11	2.8	2.16E + 11	2.0	1.06
⁹⁹ Mo	739	2.01E + 11	2.0	1.88E + 11	2.0	0.94
103 Ru	497	9.98E + 10	2.0	9.77E + 10	2.0	0.98
¹¹⁵ Cd	336	3.87E + 08	3.8	3.51E + 08	4.0	0.91
¹³² Te	228	1.44E + 11	2.8	1.39E+11	3.4	0.97
¹³⁶ Cs	1048/1048-340	2.02E + 08	2.1	1.75E + 08	16.7	0.87
¹³⁷ Cs	662	2.18E + 11	2.0	1.75E+11	5.0	0.81
¹⁴⁰ Ba	537	2.09E + 11	2.2	2.09E + 11	2.0	1.00
¹⁴¹ Ce	145	1.94E + 11	3.3	1.93E+11	2.0	1.00
¹⁴³ Ce	293	2.00E + 11	3.2	1.96E+11	2.0	0.98
¹⁴⁴ Ce	133	1.79E+11	2.4	2.09E + 11	3.0	1.16
¹⁴⁷ Nd	531	7.12E + 10	3.2	7.26E + 10	2.0	1.02
153 Sm	103/103-41	3.96E + 09	4.6	4.13E + 09	11.0	1.04
^{235}U	185	6.34E + 18	8.4	5.11E+18	5.0	0.81

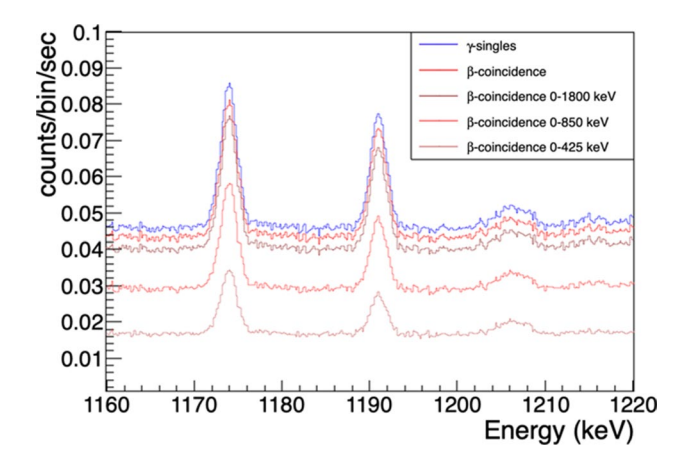
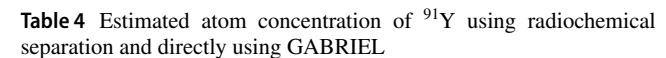


Fig. 11 Successive plots of the ⁹¹Y region with increasing beta window to the beta ungated spectrum (top)

betas. However, a more significant reduction in background can be achieved by only counting gammas associated with lower energy betas or beta gating.

The primary source of background in the energy region of ⁹¹Y gamma emission is from Compton down scattered ¹⁴⁰La 1596 keV gammas. Using an optimized beta window, peak area was reduced by 30% and background was reduced by a factor of 3.4 for an overall reduction in the MDA by a factor of 1.2. Figure 11 depicts the 1191, 1205 and 1207 keV peaks of the sum-coincidence of the 523 and 667 keV gamma-lines of ¹³²I, ⁹¹Y, and ¹³¹Te, from left to right, in the singles gamma spectrum, starting with the narrowest beta window at the bottom and successively broader beta windows upto the ungated spectrum at the top.



	MDA (atoms/g)	Measured (atoms/g)
RadChem	2.77E+08	1.89E+11
Standard HPGe	1.38E + 11	_
GABRIEL	7.52E + 10	2.05E + 11

Table 4 presents the measured result using the optimized beta window as compared to the value measured via traditional HPGe counting of the chemically separated Y fraction along with the reduction in MDA in atoms/g.

95mNb

The parent isotope, ⁹⁵Zr emits two high-intensity gammarays: 724 and 756 keV and can be readily quantified directly from singles gamma spectra. The parent-daughter activity ratio between ⁹⁵Zr/Nb is commonly used as a chronometer to estimate the time of fission. The half-life of the daughter, ⁹⁵Nb, is 34 days and can be difficult to measure at early times. The isomer daughter, ^{95m}Nb, has a much shorter half-life of 3.61 days and can be quantified using beta anti-coincidence counting. Figure 12 illustrates how the photon peak associated with ^{95m}Nb at 236 keV becomes apparent with beta anti-coincidence counting. The MDA from traditional HPGe counting to that on the GABRIEL detector was reduced from 5.26E+07 Bq to 1.48E+07 Bq, a reduction factor of 3.5 with beta anti-coincidence counting.



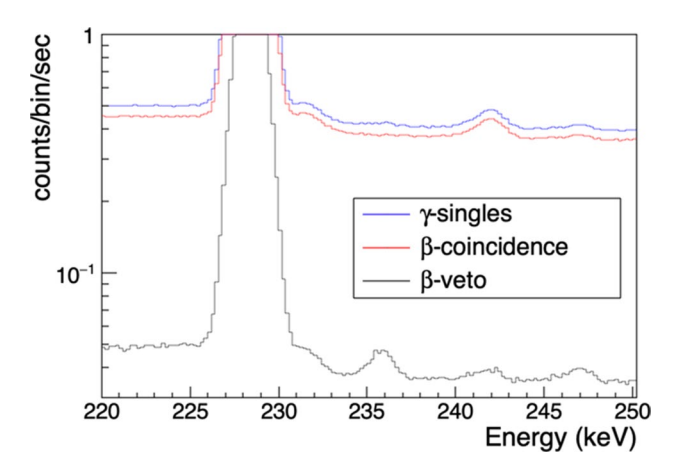


Fig. 12 Illustration of beta anti-coincidence gating on the mixed fission product spectrum and improvement to sensitivity to the 236 keV gamma-line of $^{95\text{m}}\text{Nb}$

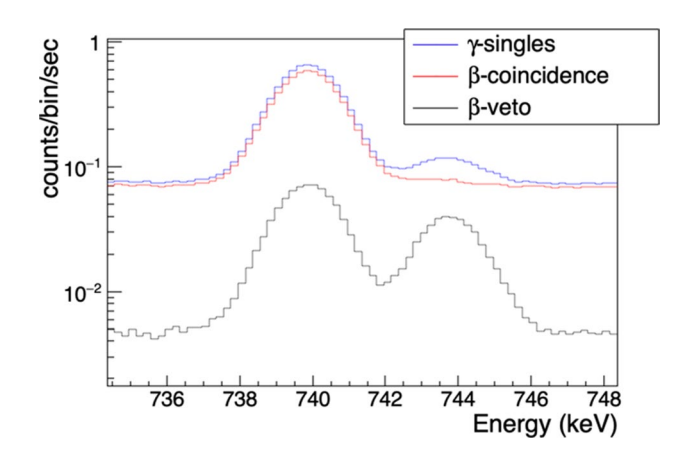


Fig. 13 Illustration of the impact of beta coincident and anti-coincident gating on the 739 keV gamma-line of ⁹⁹Mo and ⁹⁷Zr. Beta gating reduces the interference from ⁹⁷Zr on ⁹⁹Mo and anti-coincidence enhances the sensitivity to ⁹⁷Zr

97Zr/99Mo

Beta anti-coincidence improved the detection sensitivity for ⁹⁷Zr. The MDA was reduced from 1.12E + 10 to 2.74E + 9 atoms/g, a reduction factor of 3.9. The detection sensitivity for ⁹⁹Mo was improved in the beta coincidence spectrum from 7.00E + 9 to 6.49E + 9 atoms/g because of the decreased background and uncertainty in fitting the multiplet caused by the reduction in the 743 keV gamma of ⁹⁷Zr. Figure 13 depicts the beta-gated and ungated and beta anticoincidence spectrum of the 739 and 743 keV gamma-lines.

115Cd

Like ^{95m}Nb, this nuclide also highlights the value of beta anti-coincidence counting as applied to mixed fission

Table 5 Estimated concentration of ¹¹⁵Cd using radiochemical separations and directly using GABRIEL

	MDA (atoms/g)	Measured (atoms/g)
RadChem	4.76E+6	4.01E+8
Standard HPGe	3.96E + 8	_
GABRIEL	7.85E + 7	3.51E+8

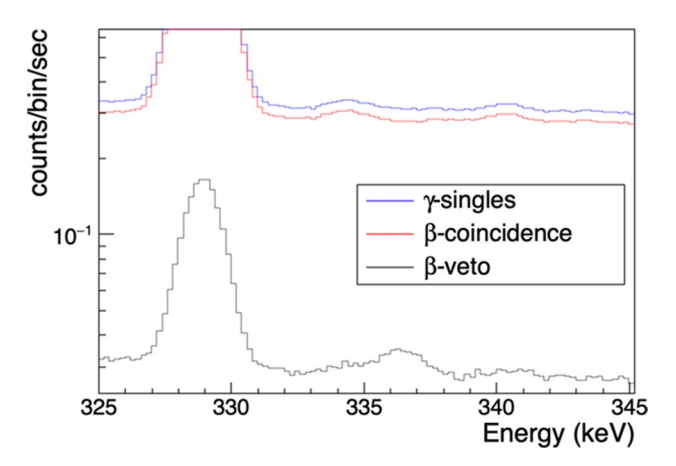


Fig. 14 Illustration of the improvement in sensitivity to In115m achieved using beta anti-coincidence counting at 336 keV

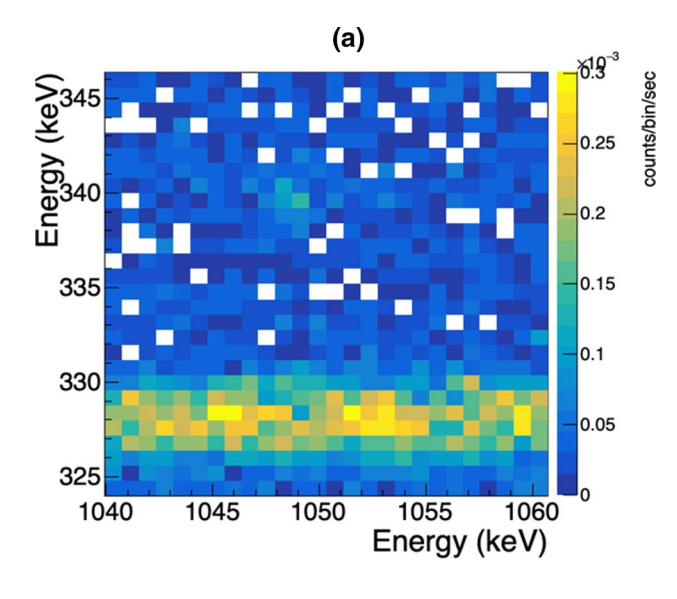
product samples. The visibility enhancement obtained using charged particle coincident gamma spectroscopy in Fig. 14. The MDA was reduced from 3.96E+8 to 7.85E+7 atoms/g, a reduction factor of 5. With beta anti-coincidence counting, ¹¹⁵Cd was successfully quantified and agreed based on a fissions/g comparison made using known fission product and their yields. Table 5 provides detection sensitivities by direct counting, GABRIEL assay, and radiochemical analysis; it is advantageous that ¹¹⁵Cd can be measured without separation in a whole solution due to its short half-life.

¹³⁶Cs

This radionuclide is a hard-to-detect fission product because of its very low yield of 5.53e-5 atoms per fission; it is also a prominent coincident gamma emitter with two high-intensity pairs, the 1048-818 and 1048-340 keV. Because of the decreasing HPGe detection efficiency as a function of energy, the 818-340 pair is the most prominent coincident feature; however, the 816 keV gamma-line from 140 La obscures the 818 in both the singles and coincident planes making the 1048-340 pair the cleanest feature to use for quantification. Figure 15 depicts the 340-1048 keV pair.

A 30–40% reduction in background can be achieved using beta coincidence counting. The primary source of background in the coincidence plane around the





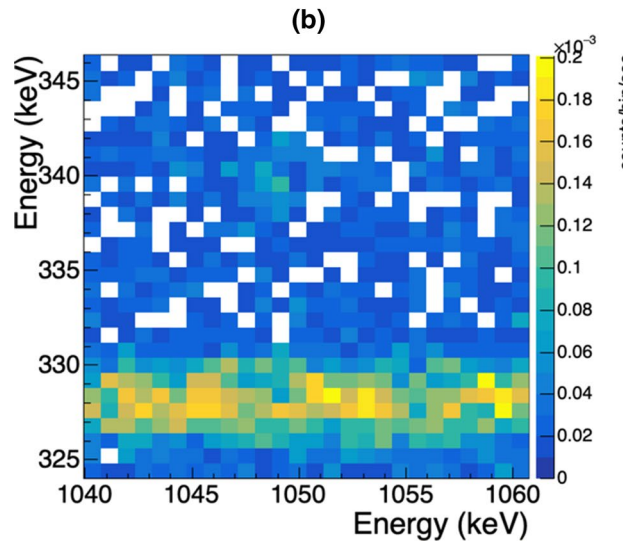


Fig. 15 Gamma-gamma coincidence plane depicting the 341/1048 keV coincidence region **a** without charged particle coincidence, and **b** with beta-coincidence and a beta-energy window. The channel space width is 1.6 keV/channel

340–1048 keV feature are the 140 La 487–1596 keV coincident events. When both the 487 and 1596 Compton scatter, the two photons are recorded within the fitting region encompassing the 136 Cs coincident feature in the coincidence plane and contribute to the peak background. The 140 La coincident gamma events are commonly associated with a $\beta_{\rm max}$ energies in excess of 1 MeV while the 136 Cs coincident events are associated with betas with a 0.34 MeV $\beta_{\rm max}$. Applying a high-energy threshold above 0.35 MeV on the betas reduces the number of observed 140 La events in this region as shown in Fig. 15. Table 6

Table 6 Estimated concentration of ¹³⁶Cs using radiochemical separation and directly using GABRIEL

	MDA (atoms/g)	Measured (atoms/g)
RadChem	6.36E+6	2.02E+8
Standard HPGe	9.64E + 7	_
GABRIEL	4.36E + 7	1.94E + 8

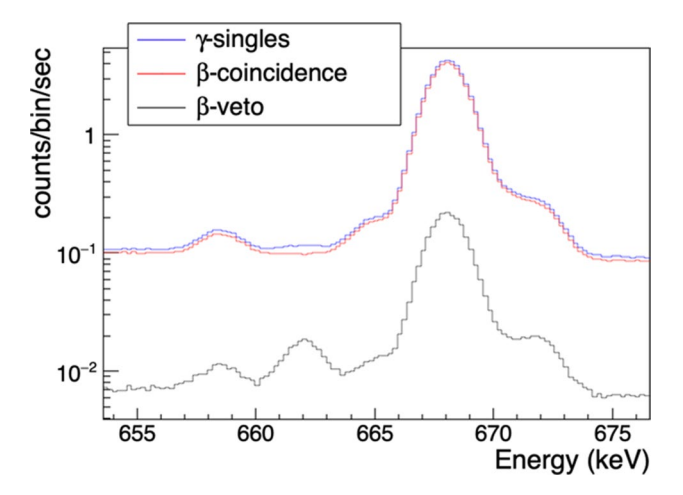


Fig. 16 Illustration of beta anti-coincidence counting improvement to sensitivity for $^{137}\mathrm{Cs}$ at 661.6 keV

Table 7 Estimated concentration of ¹³⁷Cs using radiochemical separation and directly using GABRIEL

	MDA (atoms/g)	Measured (atoms/g)
RadChem	1.19E+9	2.17E+11
Standard HPGe	4.45E + 10	_
GABRIEL	1.11E + 10	1.75E+11

depicts the improvement in detection sensitivity for ¹³⁶Cs obtained with beta-coincidence counting.

¹³⁷Cs

The MDA for 137 Cs was reduced from 4.45E+10 atoms/g in traditional HPGe counting to 1.11E+10 with the GABRIEL system, a reduction factor of 4. With beta anti-coincidence counting, this nuclide was successfully quantified and was found to be in agreement to the reference and the known fission yield of this isotope. Figure 16 illustrates the signal-to-noise enhancement for the 661.62~keV peak. Table 7 presents the reduction in the detection limit and compares quantification results from the two methods.



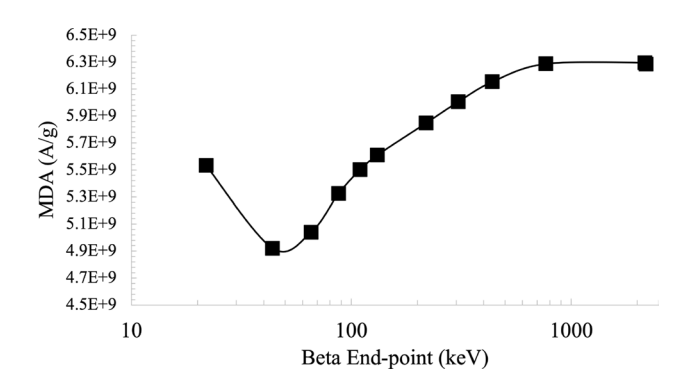


Fig. 17 Dependence of MDA on the upper beta energy window with the lower end fixed at zero

Table 8 Estimated concentration of ¹⁴⁴Ce using radiochemical separation and directly using GABRIEL

	MDA (atoms/g)	Measured (atoms/g)
RadChem	1.74E+9	1.79E+11
Standard HPGe	8.44E + 9	1.77E + 11
GABRIEL	5.04E + 9	2.09E + 11

¹⁴⁴Ce

This isotope has only one strong emission line 133 keV. This gamma is interfered with directly by the $^{140}\mathrm{Ba}$ at 132.6 keV and $^{140}\mathrm{La}$ at 131 keV. Both of these isotopes emit betas at higher energy than the β_{MAX} of $^{144}\mathrm{Ce}$. By vetoing gammas and Compton scatter associated with higher energy betas, the background surrounding this radionuclide can be reduced without impact to quantification. Figure 17 depicts the MDA as a function of the β_{MAX} cutoff applied to the measured gamma spectrum.

This isotope also has a long half-life, its specific activity at early times does not compete effectively with ¹⁴⁰Ba making the interference correction a prominent source of uncertainty when quantifying ¹⁴⁴Ce. Using beta coincidence with selective energy thresholding, both the ¹⁴⁰La/Ba background contribution can be reduced as shown in Fig. 18. The optimal detection limit based on the beta energy window was evaluated and the optimal energy cut-off was identified at 100 keV, in good agreement with the low beta end-point energy of ¹⁴⁴Ce (185 keV). Table 8 depicts the improvement in the detection sensitivity observed using the GABRIEL instrument compared to traditional singles counting (Fig. 18).

¹⁴⁷Nd

This isotope has two primary lines: 91 and 531 keV, both of which are associated with different beta energy feeding

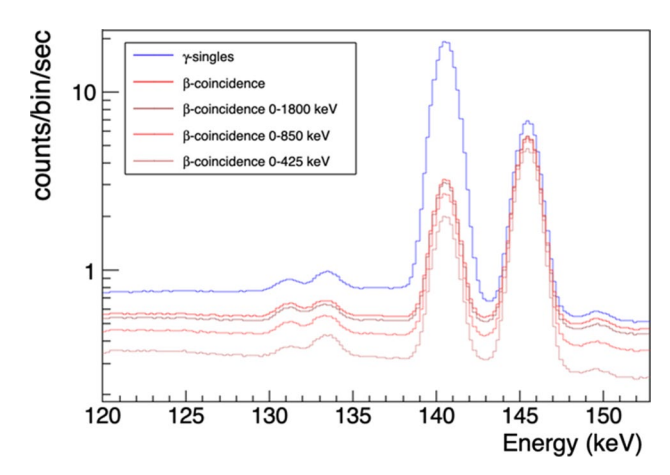


Fig. 18 Effect of varying beta window on the 133 and 137 keV gamma-lines of $^{144}\mathrm{Ce}$ and $^{140}\mathrm{Ba}$

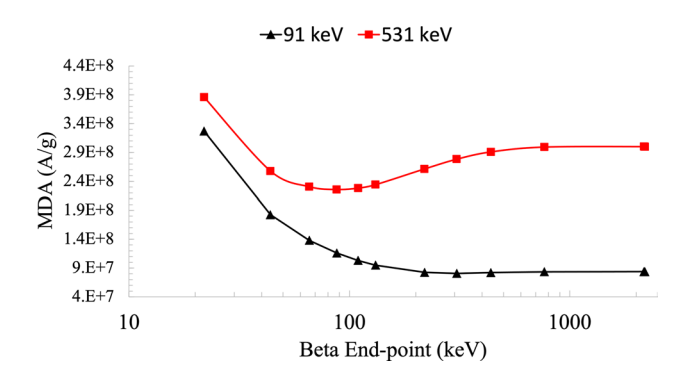


Fig. 19 Dependence of MDA on the beta energy window for 147 Nd for the 91 and 531 keV gamma-lines

Table 9 Estimated concentration of 147 Nd using radiochemical separation and directly using GABRIEL

	MDA (atoms/g)	Measured (atoms/g)
Standard HPGe	9.73E+8	7.16E+11
GABRIEL	8.07E + 7	7.26E + 11

levels. As such, they have different optimal beta windows as shown in Fig. 19.

The largest improvement in detection sensitivity for the 91 keV gamma-line ($\sim 10\%$) was immediately observed with beta gating by removing the Compton continuum associated with ^{99m}Tc. The optimal detection sensitivity was observed with a beta window spanning 0 to 700 keV producing a 2.5% reduction in peak area and a 40% reduction in background for an overall reduction in the MDA of 13%.

The improvement in the detection sensitivity of the 531 keV gamma-line was more significant relative to the



91 keV gamma-line. The optimal beta window was observed spanning 0–200 keV for a 15% reduction in peak area, a factor of 2.7 reduction in background for a 30% reduction in the MDA. Table 9 presents the improvements in the detection limit observed for the 91 keV gamma-line as compared to that of traditional HPGe spectroscopy.

¹⁵³Sm

The primary gamma energies associated with ¹⁵³Sm are correlated with beta decay. The second most prominent gammaline, 69 keV, which precedes the primary gamma at 103 keV is a prominent, K-shell electron converter such that the coincident beta can be observed with elevated energy due to the coincident conversion electron emitted in rapid proximity of the original beta. This nuclide can be measured directly from a single HPGe detector in a MFP sample using the highest intensity gamma-line at 103 keV but has high uncertainty associated with the measurement. The 102 keV interference from ^{131m}Te along with the prominent back-scatter feature produced by the 140 keV gamma-line of 99mTc make this region of the spectrum dynamic. Around the 103 keV gamma-line there is significant background, limiting the precision of the measurement and reducing confidence. The two highlighted interferences often bias the measured result from direct quantification. Figure 20 depicts the 103 keV gammaline with the accompanying 112 and 116 keV gamma-lines of ¹³²Teas observed directly from the MFP spectra.

The 103 keV peak from ¹⁵³Sm can be selectively isolated using gamma/X-ray coincidence; a better method than gamma-gamma coincidence since the 69 keV transition from the 172 keV level to the 103 keV level converts through k-shell electron emission 4.48 times more often than by direct gamma emission.

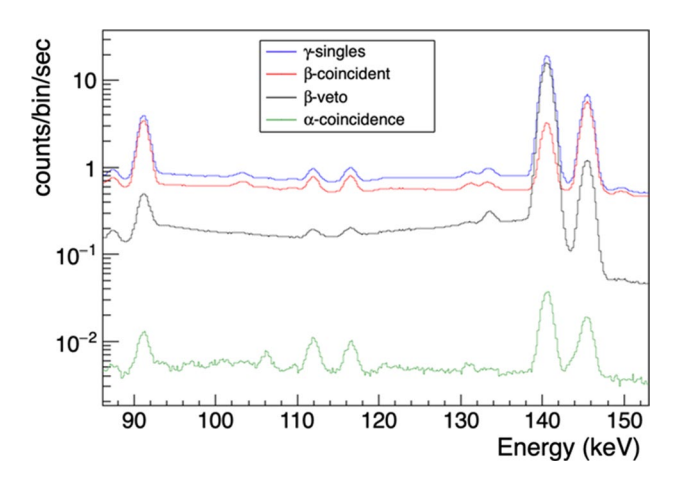
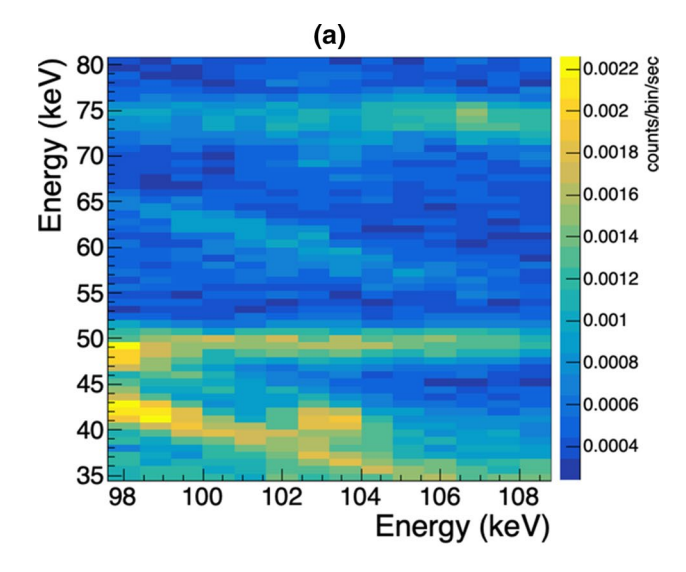


Fig. 20 Gamma spectrum of $^{153}\mathrm{Sm}$ at 103 keV and $^{132}\mathrm{Te}$ at 112 and 116 keV





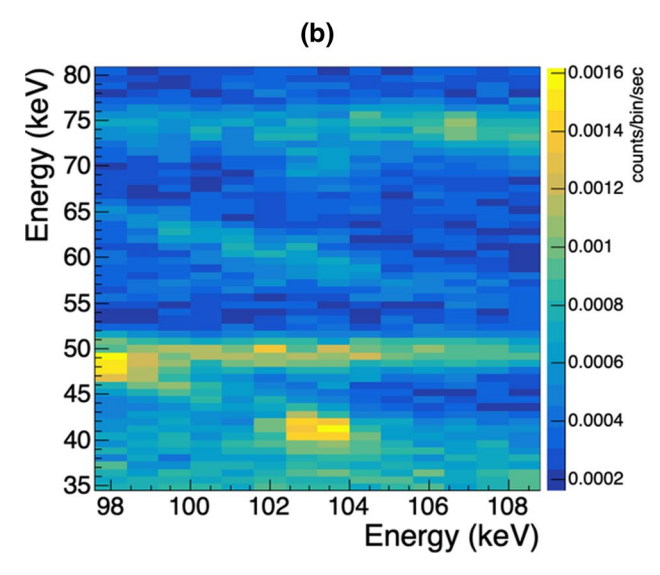


Fig. 21 Gamma-gamma coincidence plane depicting the 69/103 keV and 41/103 keV coincidence region **a** without charged particle coincidence, and **b** with beta-coincidence and a beta-energy window from 0 to 425 keV. The gamma/X-ray signature of ¹⁵³Sm is approximately 3.5 times larger than the 103/69 keV coincidence signature; however, the gamma/X-ray feature is shrouded by the 140 keV back-scatter feature without charged particle coincidence

Table 10 Estimated concentration of ¹⁵³Sm using radiochemical separation and directly using GABRIEL

	MDA (atoms/g)	Measured (atoms/g)
RadChem	4.88E+6	3.96E+9
Standard HPGe	1.04E + 9	5.16E+9
beta-coincidence	3.75E + 8	4.12E+9
γγ-coincidence + beta coincidence	4.23E+8	5.56E+9

Fig. 22 Peak-to-total ratio pulse shape discrimination plot for the LSC counter. Area below the red line and above 0.4 represents the alpha coincidence PSD cut

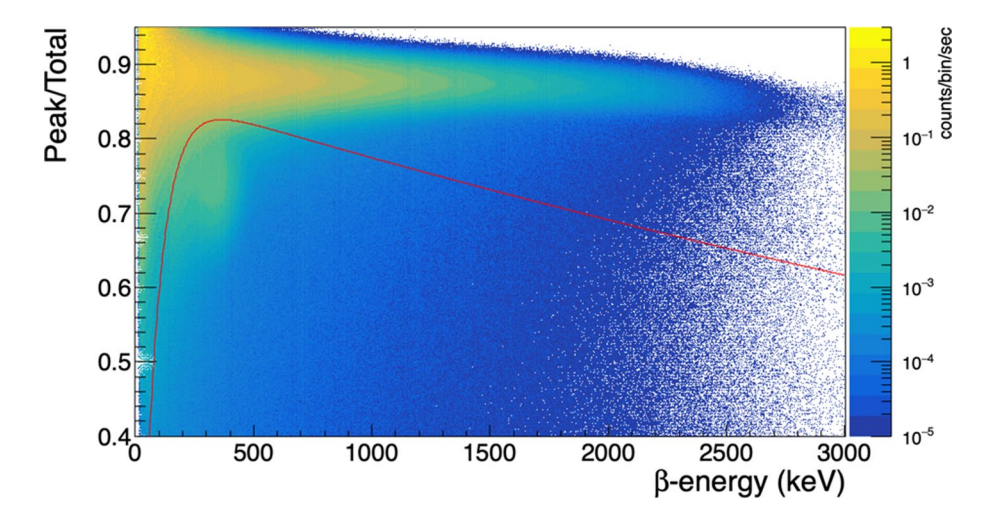


Figure 21 depicts the pure gamma-gamma spectrum neglecting the beta information and the same spectrum in coincidence with LSC. Since the ^{99m}Tc gamma is not correlated with a beta decay, the peak and associated spectral features are reduced using beta gating. This method serves as an effective way of isolating the 103 keV feature for quantification using single or coincident HPGe spectroscopy. Table 10 presents the improvement in MDA observed over standard counting when using beta coincidence with a single germanium detector and when applied to two coincident HPGe detectors.

235_[]

Charged-particle separation between alphas and betas is complicated by random summing in high-activity samples. The probability of two pulses occurring within the same window of time is proportional to the square of the count-rate if all events are Poisson random events. In this case, the count-rate observed in the liquid scintillation counter was ~ 2000 counts/s and the processing window length was 160 ns for a random sum probability of 3.2E-02%. In practice, however, the number of random sum events is closer to 0.8% because many of the observed beta decays precede delayed level transitions associated with conversion electron emission.

In cases where a subsequent conversion electron was emitted with appreciable energy > 10 keV, after-pulsing increases the tail integral clouding the area where alpha scintillation events are likely to be observed. Figure 22 depicts the peak-to-total ratio along with the threshold function used to separate the alpha and beta spectra; the events below the red line represent alpha events.

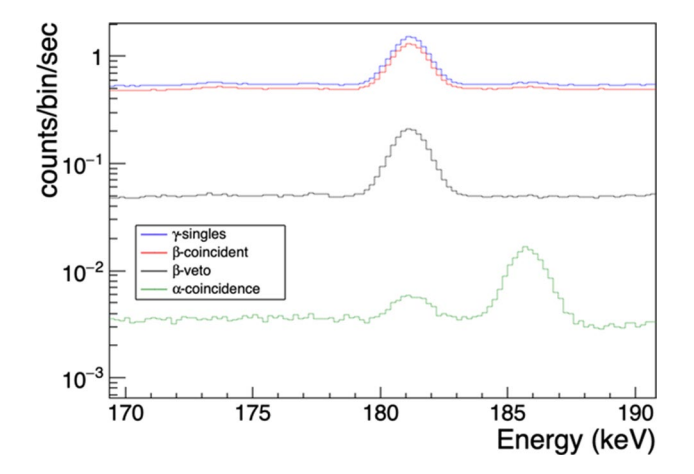


Fig. 23 Illustration of the effect of alpha coincidence gating on the 185 keV gamma-line of ²³⁵U and 181 keV gamma-line of ⁹⁹Mo

Table 11 Estimated concentration of ²³⁵U using radiochemical separation and directly using GABRIEL

	MDA (atoms/g)	Measured (atoms/g)
RadChem	1.85E+16	6.34E + 18
Standard HPGe	1.42E + 18	_
GABRIEL alpha-gated	2.37E + 17	5.11E + 18

Using the threshold shown in Fig. 22, no reduction in peak area was observed in the 185.6 keV gamma-line of ²³⁵U with a factor of 35 reduction in background or 5.9 in MDA. This translates to an atom per fission sensitivity of 27 atoms per fission. Figure 23 depicts the ungated gamma spectrum and the alpha-gated gamma spectrum for the 185.6 keV gamma-line and Table 11 compares the detection sensitivities of the various methods of analysis examined in this publication.



Conclusions

Significant improvements to the versatility and sensitivity of gamma-ray spectroscopy can be achieved for MFP samples using list-mode acquisition from a time-synchronized liquid scintillation counter. This versatility is achieved through the range of expanded analysis methodologies made available through different coincident and anticoincident analysis techniques.

This manuscript demonstrated how: (1) beta coincidence counting can help to reduce interferences in ⁹⁹Mo from ⁹⁷Zr, and ¹⁵³Sm from photon backscatter via ^{99m}Tc, (2) beta coincidence counting with select beta windows can improve detection sensitivities for radionuclides like ⁹¹Y, ¹³⁶Cs, ¹⁴⁴Ce, and ¹⁴⁷Nd, (3) alpha/beta anti-coincidence counting can be used to improve detection sensitivities for radionuclides like ⁸⁹Sr, ^{95m}Nb, ⁹⁷Zr, ¹¹⁵Cd, and ¹³⁷Cs, and (4) pulse shape separation of alphas and betas can improve detection sensitivities for alpha emitting actinides, such as ²³⁵U, by factors of 5–7.

There were limited impacts on the peak counting statistics and with improved beta detection efficiency, virtually all peak losses would be reduced or removed. In addition to the improved selectivity and spectral control afforded by the various gating techniques shown, the impacts to quantification were also limited, provided the detection efficiencies for the gamma and beta detectors were known.

Future work

As noted throughout this study, the beta detection efficiency was not comparable to a commercial liquid scintillation counter and requires optimization to attain maximum detection sensitivity. The HPGe crystals used in constructing this instrument were relatively small (~50% relative efficiency) with poor energy resolution (~3 keV FWHM @ 1332 keV) and the counting geometry, depicted in Fig. 1, was not optimized.

Based on preliminary simulation results, further reduction factors as large as an order of magnitude beyond what was achieved with this instrument may be achieved by improving the beta and gamma detection efficiencies and energy resolution of the HPGe detectors. This technique may show broader benefits in a range of applications include nuclear material safeguards characterization and spent fuel characterization in the presence of overwhelming fission product activity.

Acknowledgements Pacific Northwest National Laboratory is operated for the U.S. Department of Energy by Battelle under Contract DE-AC05-76RL01830. This work was funded by the Office of Defense Nuclear Nonproliferation Research and Development within the U.S.

Department of Energy's National Nuclear Security Administration. The views expressed here do not necessarily reflect the opinion of the United States Government, the United States Department of Energy or Pacific Northwest National Laboratory.

Funding This work is fundamental applied physics research that was performed independently, without commercial partners.

Declarations

Conflict of interest There are no conflicts of interest perpetuated or violated by the release of this manuscript.

Human or animal rights The work presented in this manuscript did not involve human or animal test subjects. Development and characterization of the presented instrument was conducted for the National Nuclear Security Administration's Domestic Nuclear Detection Office as a proof-of-concept.

References

- Wogman NA, Brodzinski RL (1973) The development and application of a beta-gamma-gamma multidimensional spectrometer. Nucl Instrum Methods 109(2): 277–283. https://doi.org/10.1016/0029-554X(73)90274-7
- Keillor ME, Aalseth Ce, Day AR, Fast JE, Hoppe EW, Hyronimus BJ, Hossbach TW, Miley HS, Seifert A, Warren GA (2009) Design and construction of an ultra-low-background 14-crystal germanium array for high efficiency and coincidence measurements. J Radioanal Nucl Chem 282(3):703–708. https://doi.org/10.1007/ s10967-009-0248-7
- 3. Kojima Y, Hayashi H, Shibata M, Endo S, Shizuma K, Taniguchi A (2011) A spectrometer for lifetime determination by β - γ - γ delayed coincidence technique at KUR-ISOL. Nucl Instrum Methods Phys Res Sect Accel Spectrom Detect Assoc Equip 659(1):193–197. https://doi.org/10.1016/j.nima.2011.08.005
- Nogami K, Yamakoshi K (1976) An extremely low background betagamma-gamma coincidence spectrometer. Nucl Instrum Methods 134(1): 519-524. https://doi.org/10.1016/0029-554X(76)90095-1
- Apalin VF, Borovoy AA, Kheruvimov AN, Kopeikin VI (1977) A low-background positron spectrometer. Nucl Instrum Methods 143(1):71–76. https://doi.org/10.1016/0029-554X(77)90333-0
- Metz LA, Payne RF, Friese JI, Greenwood LR, Kephart JD, Pierson BD (2009) Experimental measurements of short-lived fission products from uranium, neptunium, plutonium and americium. J Radioanal Nucl Chem 282(2):373–377
- Finn EC et al (2015) Cumulative fission yields of short-lived isotopes under natural-abundance-boron-carbide-moderated neutron spectrum. J Radioanal Nucl Chem. https://doi.org/10.1007/s10967-015-4085-6
- Douglas M et al (2009) Separation and quantification of chemically diverse analytes in neutron irradiated fissile materials. J Radioanal Nucl Chem 282(1):63–68
- Finn EC et al (2011) Methods to collect, compile, and analyze observed short-lived fission product gamma data. Pacific Northwest National Laboratory, Richland, WA, Formal Report PNNL-20141. Accessed 18 Feb 2014. Available: http://www.pnnl.gov/publicatio ns/abstracts.asp?report=324288
- Collins SM et al (2022) Determination of the 161Tb half-life. Appl Radiat Isot 182:110140. https://doi.org/10.1016/j.apradiso.2022. 110140
- Hyatt JE (1996) Hanford analytical services quality assurance requirements document (HASQARD). Westinghouse Hanford Co., Richland, WA



- Laustriat G (1968) The luminescence decay of organic scintillators.
 Mol Cryst 4(1-4):127-145. https://doi.org/10.1080/1542140680 8082905
- Brun R, Rademakers F (1997) ROOT—an object oriented data analysis framework. Nucl Instrum Methods Phys Res Sect Accel Spectrom Detect Assoc Equip 389(1):81–86
- 14. Gilmore G (2008) Practical gamma-ray spectrometry, 2nd edn. Wiley, Chichester

Publisher's Note Springer Nature remains neutral with regard to jurisdictional claims in published maps and institutional affiliations.

